

## Supporting Information

# Honeycomb Layered Topology Construction for Exceptional Long-wave Infrared Nonlinear Optical Crystals

Jindong Chen, Chensheng Lin, Xiaotian Jiang, Guangsai Yang, Xin Zhao, Min Luo, Bingxuan Li, Guang Peng\*, Ning Ye\*, Zhanggui Hu, Jiyang Wang, and Yicheng Wu

**Abstract:** Nonlinear optical (NLO) crystals capable of efficient long-wave infrared (8-14  $\mu\text{m}$ ) laser output remains scarce, and the superior material design of them is a momentous challenge. In this work, we develop two selenide-halides NLO crystals,  $\text{Hg}_3\text{AsSe}_4\text{Br}$  and  $\text{Hg}_3\text{AsSe}_4\text{I}$ , which are derived from honeycomb layered topology of prototype GaSe. Remarkably, they exhibit not only strong SHG effects, suitable band gap, large birefringence, broad IR transparency range and low two-photon absorption coefficients but reinforced interlayer interaction and more benign crystal growth habit, compared to those of GaSe, indicating they are promising long-wave IR NLO materials. Moreover,  $\text{Hg}_3\text{AsSe}_4\text{I}$  achieved better coexistence of comprehensive optical properties than conventional IR crystals, GaSe,  $\text{ZnGeP}_2$ , CdSe and  $\text{AgGaSe}_2$ . The idea of honeycomb layered topology design provides a chemical heuristic to explore cutting-edge IR NLO materials.

## **Table of Contents**

Experimental Procedures .....	S3-4
Table S1-11 .....	S5-10
Figure S1-10 .....	S11-15
References .....	S16-17

## Experimental Procedures

### Materials and syntheses.

HgSe (Adamas, 4N), Se (Taitan, 5N), As (Aladdin, 4N), (Taitan, 3N) and HgI<sub>2</sub> (Taitan, 3N) were used as received without further purification. The millimeter-level bulk crystals of Hg<sub>3</sub>AsSe<sub>4</sub>Br and Hg<sub>3</sub>AsSe<sub>4</sub>I with good optical quality can be easily grown by a chemical vapor transport method. A mixture of HgSe, Se, As and HgBr<sub>2</sub>/HgI<sub>2</sub> at the molar ratios of 5: 3: 2: 1 was loaded into a silica tube with an inner diameter of 12 mm and a length of 150 mm, which was then flame-sealed under vacuum and placed in a horizontal muffle furnace with a dual temperature zone. For Hg<sub>3</sub>AsSe<sub>4</sub>Br, the vaporization zone was heated to 450 °C while the crystallization zone was heated to 400 °C. For Hg<sub>3</sub>AsSe<sub>4</sub>I, the vaporization zone was heated to 380 °C while the crystallization zone was heated to 350 °C. After 3 days of annealing, it was cooled down slowly to room temperature at a rate of 5 °C/h. The dark red bulk crystals can be obtained at the crystallization zone (Figure S1), which were verified to be the title compounds by powder XRD and EDS analysis. Both Hg<sub>3</sub>AsSe<sub>4</sub>Br and Hg<sub>3</sub>AsSe<sub>4</sub>I crystals showed good air and moisture stability to be stored under ambient conditions for months without oxidation or degradation.

**Caution:** HgSe and As are toxic, so handling of these reagent requires a lot of precautions to avoid any skin contact and inhalation, and all operations should be carried out in the Ar-protected glovebox or fume cupboard.

### Single-Crystal X-Ray Diffraction.

The diffraction data were collected at room temperature on a XtaLAB Synergy R diffractometer with Mo Kα radiation ( $\lambda = 0.71073 \text{ \AA}$ ) using a  $\omega$ -scan technique. The data was reduced and integrated on CrysAlisPro program, and the absorption correction type is multi-scan.

### Powder X-Ray Diffraction.

Powder XRD patterns were obtained on a Miniflex-600 powder X-ray diffractometer with Cu Kα radiation ( $\lambda = 1.54059 \text{ \AA}$ ) at room temperature within the angular range of  $2\theta = 10\text{--}80^\circ$  with a scan step width of  $0.02^\circ$  and a fixed time of 1 s.

### EDS Elemental Analysis.

The elemental composition analysis was performed on a field emission scanning electron microscope (FESEM, SU-8010) equipped with an energy-dispersive X-ray spectroscopy (EDS).

### Thermal Analysis.

Thermogravimetric (TG) and differential thermal analysis (DTA) were performed on a NETZSCH STA 449F3 unit in N<sub>2</sub> atmosphere at 10 °C/min heating rate.

### UV-vis-NIR transmittance and absorption spectra.

The UV-vis-NIR transmittance and absorption spectra from 250 to 2500 nm, and the IR transmittance spectra from 4000 to 400 cm<sup>-1</sup> based on polished crystal wafers were recorded on a PerkinElmer Lamda-950 UV/vis/NIR spectrophotometer, and a Bruker Vertex 70 FTIR spectrophotometer, respectively. The indirect band gap value was obtained by plotting absorption spectra with Tauc function.

### Single Crystal Laser damage threshold Measurements

The laser damage thresholds (LDT) of Hg<sub>3</sub>AsSe<sub>4</sub>Br and Hg<sub>3</sub>AsSe<sub>4</sub>I single crystal was measured through single pulse measurement method. Power-tunable 1064 nm laser with pulse width  $T_p$  of 10 ns, operating frequency of 1 Hz was employed to radiate the single crystal surface with a beam spot diameter of 1.3 mm. The input laser intensities were raised from 5 mJ until the fixed size damage spot occurs, and the laser energy E was recorded. The LIDT value was calculated with the equation  $I(\text{threshold}) = E/(\pi r^2 t)$ . To ensure reliability, the LDT value was from the mean value five measured samples.

### Powder Second Harmonic Generation (SHG) Measurements.

The powder SHG measurements of AgGaS<sub>2</sub>, GaSe, Hg<sub>3</sub>AsSe<sub>4</sub>Br and Hg<sub>3</sub>AsSe<sub>4</sub>I were carried out by using a modified Kurtz and Perry method using a 2.05 μm laser radiation. All powder samples were grounded from single crystals with good quality and sieved into several distinct particle size ranges of 25–45, 45–62, 62–75, 75–109, 109–150, and 150–212 μm. Then, the samples were pressed into a 0.1-mm-thick paper ring with a diameter of 8 mm.

Powder Two-Photon Absorption (TPA) Measurements. TPA measurements was conducted on samples with particle size ranges of 150–212 μm. Power-tunable 1064 nm laser with pulse width of 10 ns, repetition frequency of 1 Hz was employed to radiate the samples surface with a beam spot size of 5 mm in diameter. The input laser intensities were tuned in the range of 5–100 MW/cm<sup>2</sup>. The SHG counts are expected to increase with the input intensity according to the square-power law as

$$I_{\text{SHG}} = aI^2 \quad (1)$$

where I is the fundamental intensity,  $I_{\text{SHG}}$  is the SHG intensity, and a is a proportionality constant that is dependent on  $\chi(2)$ . However, when the band gaps of tested crystals are all less than twice (2.33 eV) that of the fundamental excitation photon energy ( $h\nu = 1.165 \text{ eV}$ ), two photon absorption (TPA) phenomenon will be remarkable and become the main mechanism for optical damage, which can be fitted using equation S2

$$I_{\text{SHG}} = a\left(\frac{I}{1 + \beta Id}\right)^2 \quad (2)$$

where  $I$  is the fundamental intensity,  $\beta$  is the TPA coefficient,  $d$  is average particle size of  $181\text{ }\mu\text{m}$  and  $a$  is a proportionality constant that incorporates  $\chi(2)$ . All input intensity-dependent SHG intensity data under  $1064\text{ nm}$  laser of tested crystals can be fitted by equation S2, and the SHG fit curves were plotted using equation S1, where a value was obtained from TPA fit.

#### **Computational method.**

First-principles calculations based on the density functional theory (DFT) were performed to analyze the electronic structure, optical properties, and density of states (DOS) by the plane wave pseudopotential method implemented in the CASTEP package.[1] The valence electrons of component elements were Hg 5d106s2, As 4s24p3, Se 4s24p4, Br 4s24p5 and I 5s25p5. The generalized gradient approximation (GGA) in the Perdew–Burke–Eruzerhof (PBE) scheme [2] was used to describe the exchange and correlative potential of electron–electron interactions. A Monkhorst–Pack [3] grid size for SCF calculation is  $2 \times 2 \times 2$  was used in the first Brillouin zone of the unit cell. The plane wave basis set cut-off is  $450\text{ eV}$ . 72 empty bands were utilized for optics parameters calculation, and scissors operators of  $0.645\text{ eV}$  and  $0.523\text{ eV}$  for  $\text{Hg}_3\text{AsSe}_4\text{Br}$  and  $\text{Hg}_3\text{AsSe}_4\text{I}$  were applied to move the simulated band gap to the right place. The second-order nonlinear susceptibility was calculated through the “velocity-gauge” formula,[4] and the SHG density was calculated by a band-resolved method.[5] The Bader charge analysis[6] was used to decompose every energy band to the component ions, so the percentage of each component ion in the energy band was obtained and also the ionic contribution to the SHG coefficients can be obtained by summation of all energy bands.

## Results and Discussion

**Table S1** Crystallographic Data and Refinement Details for  $\text{Hg}_3\text{AsSe}_4\text{Br}$  and  $\text{Hg}_3\text{AsSe}_4\text{I}$

Formula	$\text{Hg}_3\text{AsSe}_4\text{Br}$	$\text{Hg}_3\text{AsSe}_4\text{I}$
CCDC number	2183986	2183985
Formula weight (amu)	1072.42	1119.43
Temp. (K)	293(2)	293(2)
$\lambda(\text{\AA})$	0.71073	0.71073
Crystal system	Hexagonal	Hexagonal
Space group	$P6_3mc$	$P6_3mc$
$a$ (\text{\AA})	7.7139(5)	7.7054(4)
$b$ (\text{\AA})	7.7139(5)	7.7054(4)
$c$ (\text{\AA})	9.4846(10)	10.0008(9)
$\alpha$ (deg)	90	90
$\beta$ (deg)	90	90
$\gamma$ (deg)	120	120
$V$ (\text{\AA}^3)	488.76(8)	514.23(7)
$Z$	2	2
$\rho_{\text{calc}}$ (g/cm <sup>3</sup> )	7.287	7.230
$\mu$ (mm <sup>-1</sup> )	69.261	64.948
$F$ (000)	888	924
Reflections collected/unique	1851 / 456	2182 / 492
Completeness	99.5	100
$R_{\text{int}}$	0.0550	0.0382
$R_1$ ( $I > 2\sigma(I)$ )	0.0381	0.0238
wR <sub>2</sub> ( $I > 2\sigma(I)$ )	0.0701	0.0464
$R_1$ (all data)	0.0359	0.0286
wR <sub>2</sub> (all data)	0.0717	0.0474
Flack parameter	0.00(3)	0.010(15)
GOOF on $F^2$	0.995	0.980

**Table S2** Atomic Coordinates ( $\times 10^4$ ) and Equivalent Isotropic Displacement Parameters ( $\text{\AA}^2 \times 10^3$ ).

Atom	x	y	z	U(eq)
$\text{Hg}_3\text{AsSe}_4\text{Br}$				
Hg	4966(1)	5034(1)	-70(2)	28(1)
Br	6667	3333	2140(4)	23(1)
Se1	8500(1)	6999(3)	-1253(3)	16(1)
Se2	3333	6667	1344(4)	16(1)
As	10000	10000	147(5)	16(1)
$\text{Hg}_3\text{AsSe}_4\text{I}$				
Hg	5036(1)	4964(1)	4929(1)	28(1)
I	6667	3333	2152(2)	18(1)
Se1	6667	3333	6292(3)	16(1)
Se2	6976(2)	8488(1)	3743(2)	15(1)
As	10000	10000	5057(4)	14(1)

**Table S3** Selected bond lengths ( $\text{\AA}$ ) and angles (degree).

	$\text{Hg}_3\text{AsSe}_4\text{Br}$		$\text{Hg}_3\text{AsSe}_4\text{I}$
Hg-Se1	2.618(2)	Hg-Se1	2.6372(15)
Hg-Se2	2.561(3)	Hg-Se2	2.568(2)
As-Se1	2.405(4)	As-Se1	2.408(3)
Se1-Hg-Se1	108.21(13)	Se1-Hg-Se1	103.57(11)
Se1-Hg-Se2	124.42(4)	Se1-Hg-Se2	125.33(3)
Se1-As-Se1	92.43(18)	Se1-As-Se1	93.06(16)

**Table S4** Anisotropic Displacement Parameters ( $\text{\AA}^2 \times 10^3$ ).The Anisotropic displacement factor exponent takes the form:  $-2\pi^2[h^2a^{*2}U_{11}+2hka^{*}b^{*}U_{12}+\dots]$ .

Atom	$U_{11}$	$U_{22}$	$U_{33}$	$U_{23}$	$U_{13}$	$U_{12}$
$\text{Hg}_3\text{AsSe}_4\text{Br}$						
Hg	21(1)	21(1)	42(1)	-5(1)	5(1)	10(1)
Br	28(1)	28(1)	13(2)	0	0	14(1)
Se1	16(1)	12(1)	18(1)	0(1)	0(1)	6(1)
Se2	18(1)	18(1)	12(2)	0	0	9(1)
As	15(1)	15(1)	16(3)	0	0	8(1)
$\text{Hg}_3\text{AsSe}_4\text{I}$						
Hg	18(1)	18(1)	48(1)	4(1)	-4(1)	9(1)
I	20(1)	20(1)	14(1)	0	0	10(1)
Se1	15(1)	15(1)	16(2)	0	0	8(1)

Se2	9(1)	12(1)	22(1)	0(1)	-1(1)	4(1)
As	12(1)	12(1)	18(2)	0	0	6(1)

**Table S5** The dipole moment (Debye) of groups in unit cell

Groups	BVS	u <sub>x</sub>	u <sub>y</sub>	u <sub>z</sub>
$\text{Hg}_3\text{AsSe}_4\text{I}$				
$[\text{HgSe}_3]_1 \times 2$	2.06	0	-1.37285270	4.557803046
$[\text{HgSe}_3]_2 \times 2$	2.06	-1.184517477	0.683909429	4.561544906
$[\text{HgSe}_3]_3 \times 2$	2.06	1.187842831	0.688281191	4.557875796
$[\text{AsSe}_3] \times 2$	2.970	0	0	7.492338795
Total		0	0	42.34
$\text{Hg}_3\text{AsSe}_4\text{Br}$				
$[\text{HgSe}_3]_1 \times 2$	2.13	0	1.486245924	4.342920602
$[\text{HgSe}_3]_2 \times 2$	2.13	-1.283726428	0.742381456	4.345324599
$[\text{HgSe}_3]_3 \times 2$	2.13	1.288608352	0.74559793	4.33631859
$[\text{AsSe}_3] \times 2$	2.998	0	0	7.329122382
Total		0	0	40.71

**Table S6** Calculated values of  $g_{ijk}$  and C

Compounds	Groups	$g_{ijk}$	C
$\text{ZnGeP}_2$	$\text{ZnP}_4$	$g_{123}=0.999$	0.999
	$\text{GeP}_4$	$g_{123}=0.999$	
AgGaSe <sub>2</sub>	$\text{AgSe}_4$	$g_{123}=0.98425$	0.9828
	$\text{GaSe}_4$	$g_{123}=0.98133$	
GaSe	$\text{Ga}_2\text{Se}_6$	$g_{222}=0.998$	0.998
HASI	$\text{HgSe}_3$	$g_{311}=0.6255$	0.719
	$\text{AsSe}_3$	$g_{311}=1$	
HASB	$\text{HgSe}_3$	$g_{311}=0.6413$	0.731
	$\text{AsSe}_3$	$g_{311}=1$	

**Table S7** The ionic contribution to the SHG coefficient by Bader charge analysis

	Hg	As	Se	I/Br
<b>HASI</b>				
$d_{31}$	28.09	9.22	44.72	17.97
$d_{33}$	27.51	9.78	45.68	17.03
<b>HASB</b>				
$d_{31}$	28.18	10	46.82	15.0

$d_{33}$	27.47	11.21	47.68	13.64
----------	-------	-------	-------	-------

**Table S8** The binding energy of  $[Hg_3AsSe_4]$  single layer and cohesive energy of interlayer.

	Binding energy (BE, eV)	Cohesive energy (CE, eV)	BE/CE ratio
HASI	-1.859	-1.007	1.846
HASB	-2.469	-1.106	2.232
GaSe	-8.511	-0.199	42.77

**Table S9.** The properties comparison between  $Hg_3AsSe_4X$  ( $X = Br$  and  $I$ ) and reported NLO selenides.

Selenides	$d_{ij}$ (pm/V)	Eg (eV)	$\Delta n$	Reference
$Hg_3AsSe_4I$	62.8	2.13	0.36	This work
$Hg_3AsSe_4Br$	43.1	2.10	0.37	This work
GaSe	54	2.0	0.4	1
$AgGaSe_2$	33	1.83	0.02	2
$LiInSe_2$	12.5	2.83	0.05	3
CdSe	36	1.7	0.02	4
$AgGaGe_5Se_{12}$	34	2.14	0.15	5
$AgGaGeSe_4$	33	2.27	0.03	6
$BaGa_4Se_7$	20.5	2.64	0.08	7
$BaGa_2GeSe_6$	23.6	2.31	0.15	8
$\beta-BaGa_2Se_4$	~10	2.49	0.18	9
$\beta-BaGa_4Se_7$	37.97	2.82	0.04	10
$\beta-LiGaSe_2$	~20	1.71	0.033	11
$MgGa_2Se_4$	-20.07	2.96	0.048	12
$Na_{0.5}K_{0.5}AsSe_2$	22.50	1.78	N/A	13
$NaMg_3Ga_3Se_8$	9.3	2.77	0.072	14
$Ba_2As_2Se_5$	53.60	1.43	N/A	15
$NaGa_3Se_5$	6.61	2.62	0.05	16
$NaIn_3Se_5$	9.33	2.17	0.004	17
$Li_2In_2GeSe_6$	-8.3	2.27	0.043	18
$LiGaGe_2Se_6$	18.6	2.38	0.04	19
$Li_2CdSnSe_4$	12.5	2.2	N/A	20
$Li_2ZnSnSe_4$	12	2.0	N/A	21
$Na_4MgGe_2Se_6$	-24.9	2.53	0.09	22
$BaHgSe_2$	26.52	1.56	0.1473	23
$Na_2BaGeSe_4$	10.69	2.46	0.026	24
$Na_2BaSnSe_4$	12.25	2.25	0.011	24
$BaCu_2GeSe_4$	5.62	1.88	N/A	25
$BaCu_2SnSe_4$	12.65	1.72	N/A	25
$Li_2BaSnSe_4$	9.64	2.18	0.066	26
$Li_2BaGeSe_4$	14.17	2.40	0.038	26
$SrZnSnSe_4$	30.03	1.82	0.290	27
$Ba_6In_6Zn_4Se_{19}$	16.3	2.2	0.098	28

<chem>Na2ZnSn2Se6</chem>	23.7	2.05	0.075	29
<chem>Na2CdSn2Se6</chem>	20.3	2.15	0.044	29
<chem>Ba12In12Zn8Se38</chem>	22.9	2.15	0.043	30
<chem>(K0.38Ba0.81)Ga2Se4</chem>	9.1	2.03	0.21	31
<chem>BaHgGeSe4</chem>	-31.7	2.49	~0.1	32
<chem>Li4HgSn2Se7</chem>	-20.07	2.10	0.035	33
<chem>Rb4Ge4Se12</chem>	48.7	2.1	N/A	34
<chem>RbInSn2Se6</chem>	60.2	1.8	0.067	35
<chem>CsGaSn2Se6</chem>	53.3	1.87	0.053	36
<chem>CsCd4Ga5Se12</chem>	~43	2.21	0.014	37

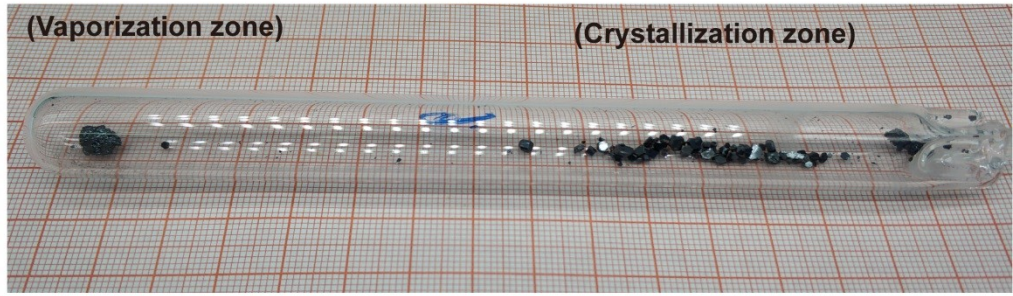
**Table S10** Comparison of key physical parameters.

Compounds	ZnGeP <sub>2</sub>	AgGaSe <sub>2</sub>	GaSe	HASB	HASI
E <sub>g</sub> (eV)	1.9	1.83	2.0	2.10	2.13
d <sub>ij</sub> (pm/V)	75	33	54	43.1	62.8
PSHG ( $\times$ AgGaS <sub>2</sub> )	--	--	7.5	6.2	8.8
Δn	0.04	0.03	~0.4	0.37	0.36
IR range (μm)	0.74–12.5	0.71-19	0.62-19	0.6-19	0.6-19
BE/CE	--	--	42.77	2.232	1.846
Dipole moment (Debye)	0	0	0	40.7	42.3
Structural factor C	0.999	0.983	0.998	0.731	0.719
TPA coeff. (cm/GW)	34.3	42.2	26.2	11.1	9.2

**Table S11** LDT values of measured samples.

sample	input laser intensity (mJ)	LDT (MW/cm <sup>2</sup> )
HASB		
Sample1	15	113.0
Sample2	12	90.4
Sample3	12	90.4
Sample4	13	98.0
Sample5	10	75.4
Mean value		93.4
HASI		
Sample1	17	128.1
Sample2	15	113.0
Sample3	16	120.6
Sample4	15	113.0
Sample5	12	90.4
Mean value		113.0

(a)



(b)

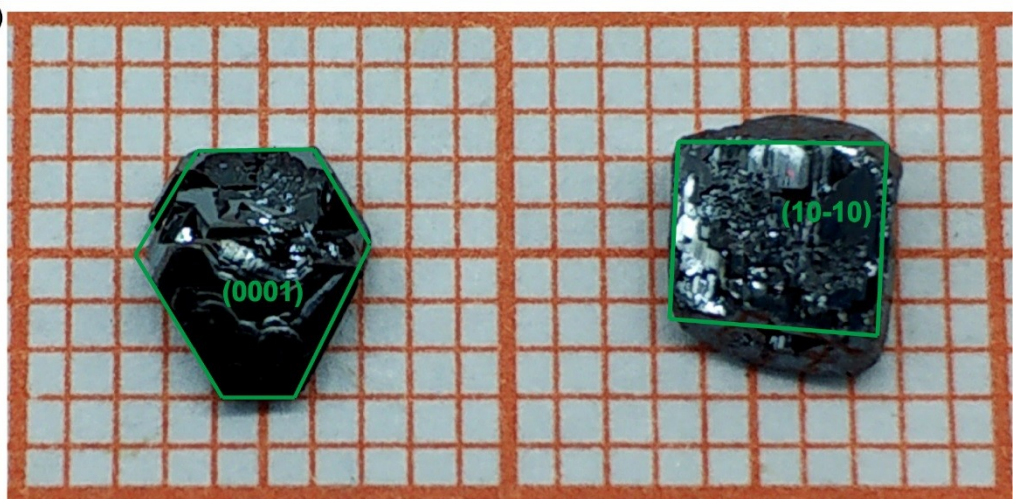
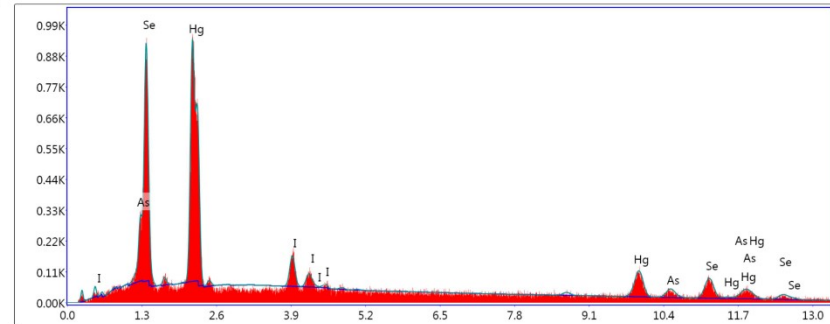


**Figure S1** (a) Chemical vapor transport crystal growth in muffle furnace with a dual temperature zone and (b) as-grown single crystal of HASI with (0001) and (10-10) preferred growth planes.

(a)



(b)

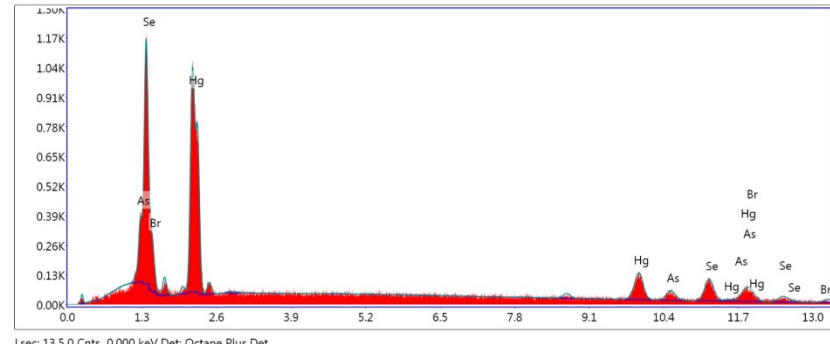


**Figure S2** Energy-dispersive X-ray Spectroscopy analysis of HASI (a) and HASB (b).

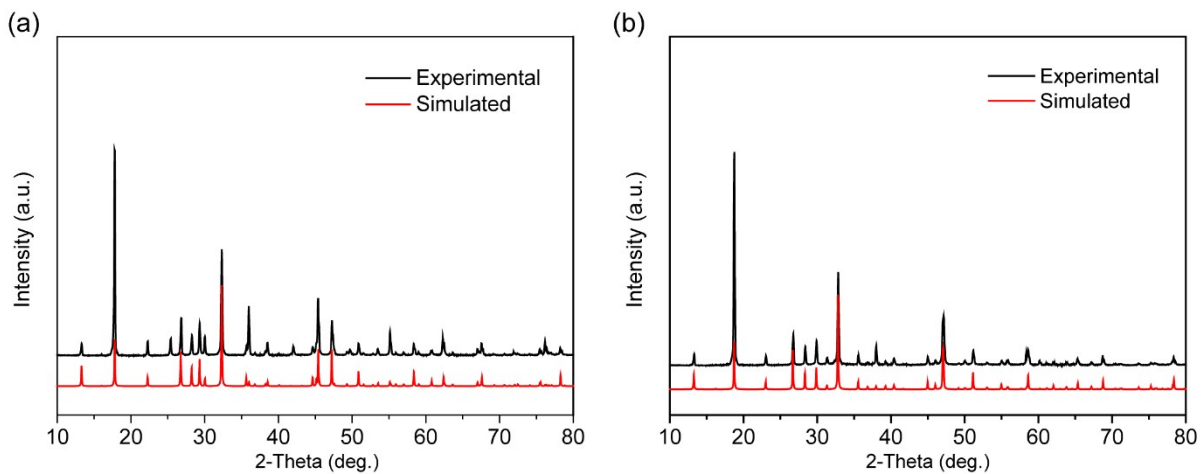


**Figure S3** Powder XRD patterns of the experimental and simulated for HASI (a) and HASB (b).

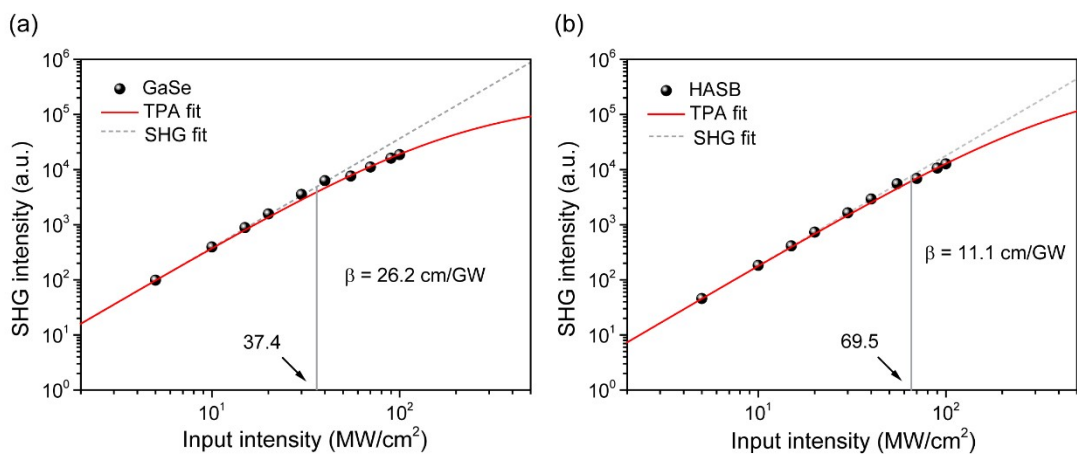


**Figure S4** Log–log plots of input intensity-dependent SHG intensity under 1064nm laser for GaSe (a) and HASB (b).

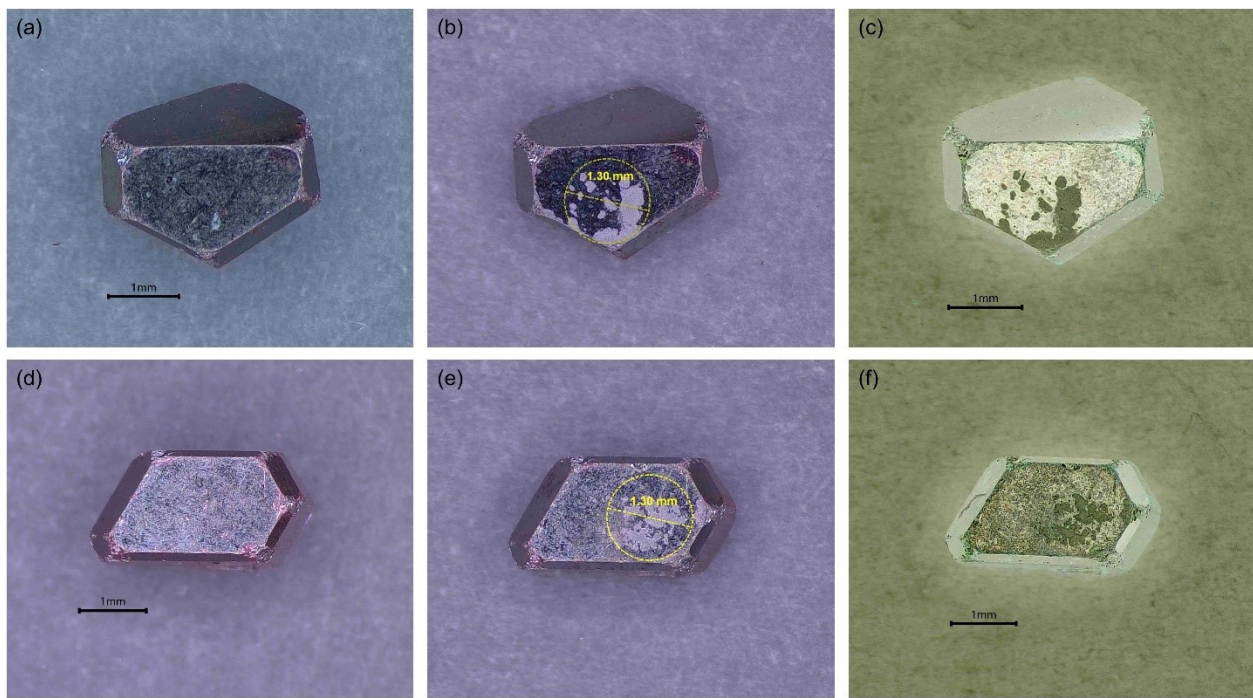


**Figure S5** Schematic photographs of pristine single crystal, crystal after laser damage, and negative film of HASI (a, b and c) and HASB (d, e and f) for laser damage threshold measurements.

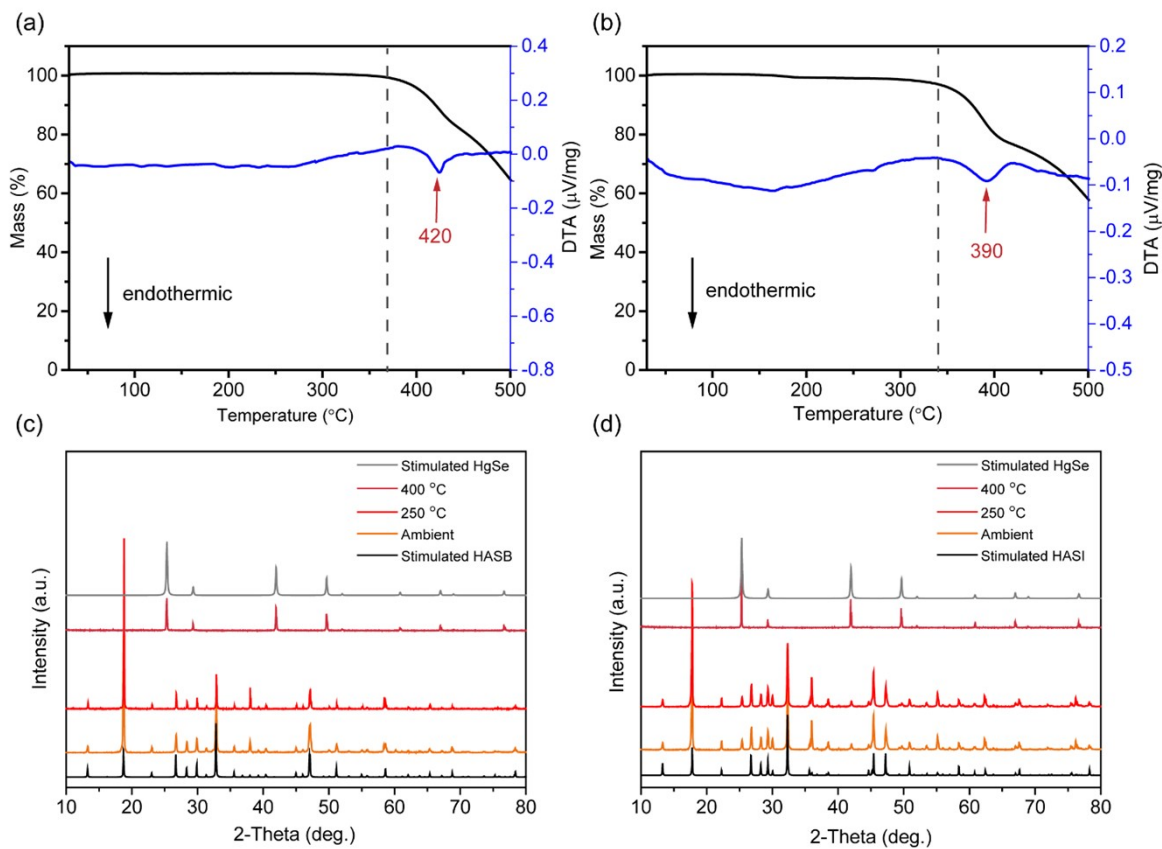


**Figure S6** TG-DTA curves of HASB (a) and HASI (b). various-temperature XRD patterns of HASB (c) and HASI (d).

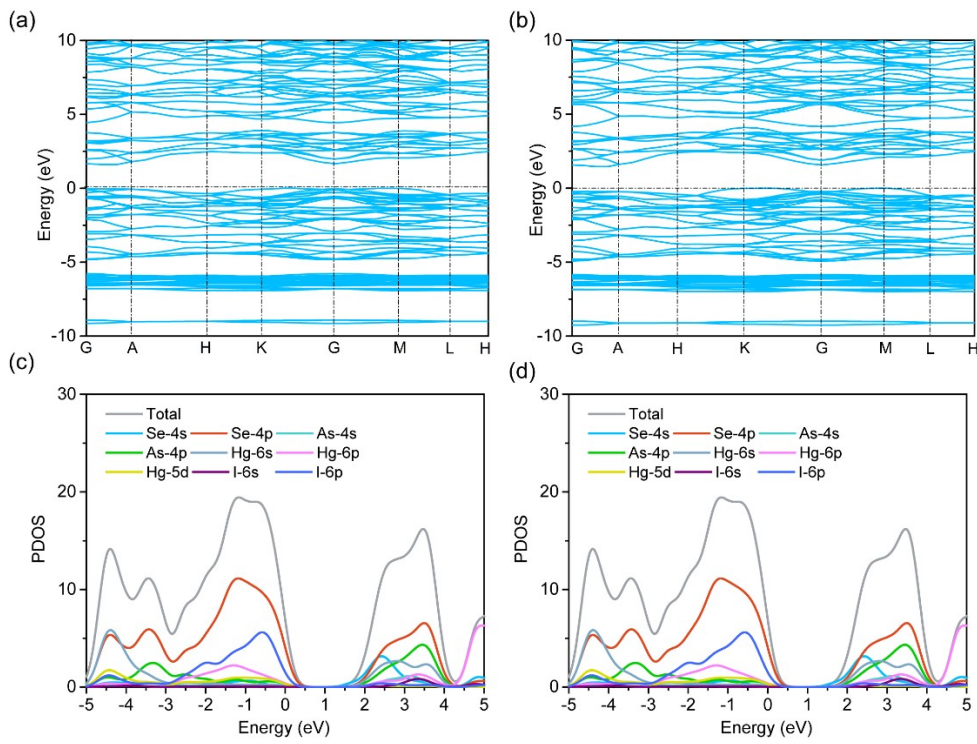


**Figure S7** Band structure of HASI (a) and HASB (b), and PDOS of HASI (c) and HASB (d).

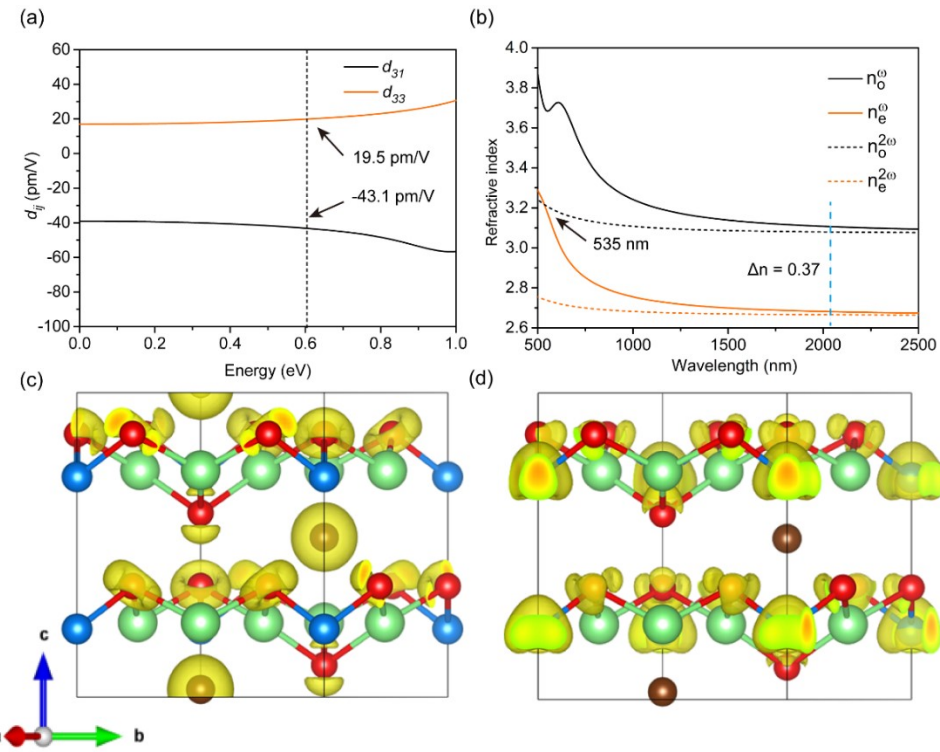


**Figure S8** Calculated frequency-dependent SHG coefficients (a), Calculated refractive index dispersion curves, and  $d_{31}$  SHG density of occupied (c) and unoccupied (d) electronic state of  $Hg_3AsSe_4Br$ .

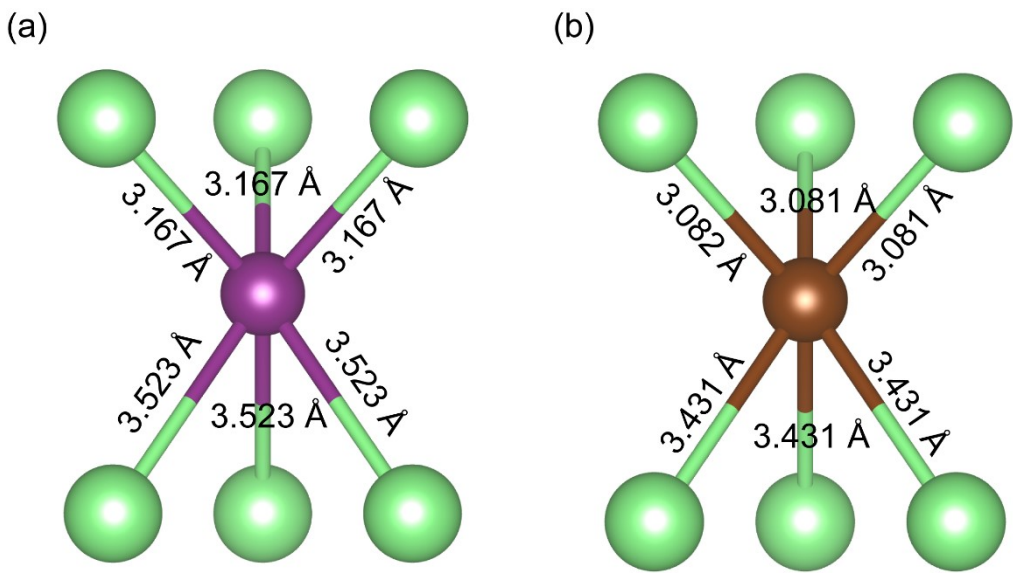


**Figure S9** The coordination environment of I and Br atoms.

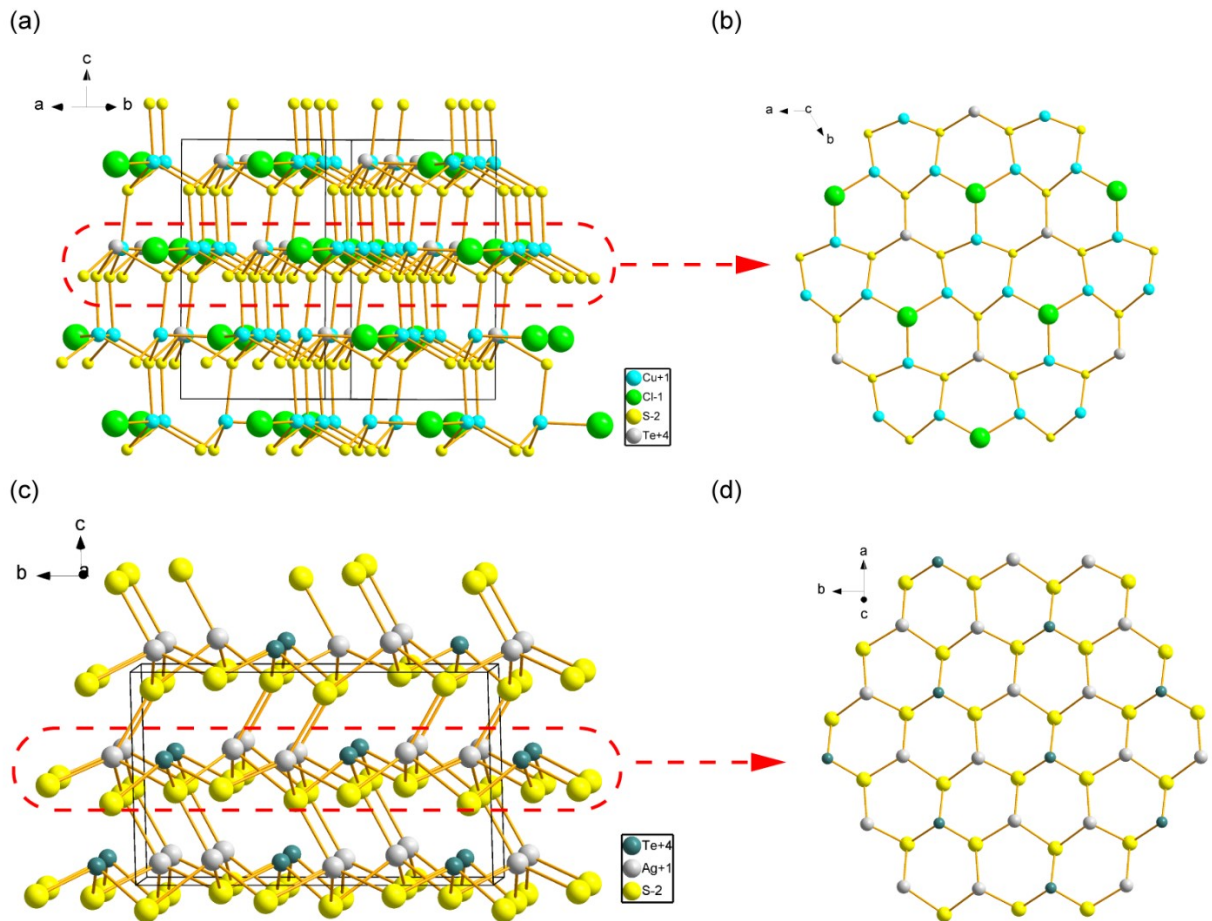


**Figure S10.** Crystal structure and honeycomb layered topology of  $\text{Cu}_3\text{TeS}_3\text{Cl}$  (a, b),  $\text{Ag}_2\text{TeS}_3$  (c, d)

## References

- (1) a) J. C. Stewart, D. S. Matthew, J. P. Chris, J. H. Phil, I. J. P. Matt, R. Keith, C. P. Mike, *Z. Kristallogr. - Cryst. Mater.* **2005**, 220, 567; b) W. Kohn, L. J. Sham, *Phys. Rev.* **1965**, 140, A1133.
- (2) a) J. P. Perdew, K. Burke, M. Ernzerhof, *Phys. Rev. Lett.* **1996**, 77, 3865; b) J. P. Perdew, Y. Wang, *Phys. Rev. B* **1992**, 46, 12947.
- (3) H. J. Monkhorst, J. D. Pack, *Phys. Rev. B* **1976**, 13, 5188.
- (4) a) W.-D. Cheng, C.-S. Lin, H. Zhang, G.-L. Chai, *J. Phys. Chem. C* **2018**, 122, 4557-4564; b) J. Chen, H. Chen, F. Xu, L. Cao, X. Jiang, S. Yang, Y. Sun, X. Zhao, C. Lin, N. Ye, *J. Am. Chem. Soc.* **2021**, 143, 10309-10316.
- (5) M.-H. Lee, C.-H. Yang, J.-H. Jan, *Phys. Rev. B* **2004**, 70, 235110.
- (6) C.-S. Lin, A.-Y. Zhou, W.-D. Cheng, N. Ye, G.-L. Chai, *J. Phys. Chem. C* **2019**, 123, 31183-31189.
- (7) J. Yao, W. Yin, K. Feng, X. Li, D. Mei, Q. Lu, Y. Ni, Z. Zhang, Z. Hu, Y. Wu, *J. Cryst. Growth* **2012**, 346, 1-4.
- (8) K. Kato, V. V. Badikov, L. Wang, V. L. Panyutin, K. V. Mitin, K. Miyata, V. Petrov, *Opt. Lett.* **2020**, 45, 2136-2139.
- (9) Y. Zhang, Q. Bian, H. Wu, H. Yu, Z. Hu, J. Wang, Y. Wu, *Angew. Chem. Int. Ed.* **2022**, 61, e202115374.
- (10) Z. Qian, Q. Bian, H. Wu, H. Yu, Z. Lin, Z. Hu, J. Wang, Y. Wu, *J. Mater. Chem. C* **2022**, 10, 96-101.
- (11) P. Wang, Y. Chu, A. Tudi, C. Xie, Z. Yang, S. Pan, J. Li, *Adv. Sci.* **2022**, 9, e2106120.
- (12) W. Cai, A. Abudurusuli, C. Xie, E. Tikhonov, J. Li, S. Pan, Z. Yang, *Adv. Funct. Mater.* **2022**, 32, 2200231
- (13) A. K. Iyer, J. B. Cho, H. R. Byun, M. J. Waters, S. Hao, B. M. Oxley, V. Gopalan, C. Wolverton, J. M. Rondinelli, J. I. Jang, M. G. Kanatzidis, *J. Am. Chem. Soc.* **2021**, 143, 18204-18215.
- (14) K. Wu, Z. Yang, S. Pan, *Inorg. Chem.* **2015**, 54, 10108-10110.
- (15) A. K. Iyer, J. B. Cho, M. J. Waters, J. S. Cho, B. M. Oxley, J. M. Rondinelli, J. I. Jang, M. G. Kanatzidis, *Chem. Mater.* **2022**, 34, 5283-5293.
- (16) Q. T. Xu, S. S. Han, J. N. Li, S. P. Guo, *Inorg. Chem.* **2022**, 61, 5479-5483.
- (17) S.-F. Li, X.-M. Jiang, B.-W. Liu, D. Yan, C.-S. Lin, H.-Y. Zeng, G.-C. Guo, *Chem. Mater.* **2017**, 29, 1796-1804.
- (18) A. P. Yelisseyev, M. S. Molokeev, X. Jiang, P. G. Krinitzin, L. I. Isaenko, Z. Lin, *J. Phys. Chem. C* **2018**, 122, 17413-17422.
- (19) A. P. Yelisseyev, L. I. Isaenko, P. Krinitzin, F. Liang, A. A. Goloshumova, D. Y. Naumov, Z. Lin, *Inorg. Chem.* **2016**, 55, 8672-8680.
- (20) J.-H. Zhang, D. J. Clark, A. Weiland, S. S. Stoyko, Y. S. Kim, J. I. Jang, J. A. Aitken, *Inorg. Chem. Frontiers* **2017**, 4, 1472-1484.
- (21) J. H. Zhang, D. J. Clark, J. A. Brant, C. W. Sinagra, 3rd, Y. S. Kim, J. I. Jang, J. A. Aitken, *Dalton Trans.* **2015**, 44, 11212-11222.
- (22) K. Wu, Z. Yang, S. Pan, *Inorg. Chem.* **2015**, 54, 10108-10110.
- (23) C. Li, W. Yin, P. Gong, X. Li, M. Zhou, A. Mar, Z. Lin, J. Yao, Y. Wu, C. Chen, *J. Am. Chem. Soc.* **2016**, 138, 6135-6138.
- (24) K. Wu, Z. Yang, S. Pan, *Angew. Chem. Int. Ed.* **2016**, 55, 6713-6715.
- (25) L. Nian, J. Huang, K. Wu, Z. Su, Z. Yang, S. Pan, *RSC Adv.* **2017**, 7, 29378-29385.
- (26) F. Hou, D. Mei, Y. Zhang, F. Liang, J. Wang, J. Lu, Z. Lin, Y. Wu, *J. Alloy. Compd.* **2022**, 904, 163944.
- (27) K. Wu, B. Zhang, Z. Yang, S. Pan, *J. Am. Chem. Soc.* **2017**, 139, 14885-14888.
- (28) A. Zhou, C. Lin, B. Li, W. Cheng, Z. Guo, Z. Hou, F. Yuan, G.-L. Chai, *J. Mater. Chem. C* **2020**, 8, 7947-7955.
- (29) R. Ye, X. Cheng, B.-W. Liu, X.-M. Jiang, L.-Q. Yang, S. Deng, G.-C. Guo, *J. Mater. Chem. C* **2020**, 8, 1244-1247.

- (30) L.-Q. Yang, R. Ye, X.-M. Jiang, B.-W. Liu, H.-Y. Zeng, G.-C. Guo, *J. Mater. Chem. C* **2020**, *8*, 3688-3693.
- (31) Y. N. Li, Y. Chi, Z. D. Sun, H. Xue, N. T. Suen, S. P. Guo, *Chem. Commun. (Camb)* **2019**, *55*, 13701-13704.
- (32) Y. Guo, F. Liang, W. Yin, Z. Li, X. Luo, Z.-S. Lin, J. Yao, A. Mar, Y. Wu, *Chem. Mater.* **2019**, *31*, 3034-3040.
- (33) Y. Guo, F. Liang, Z. Li, W. Xing, Z. Lin, J. Yao, Y. Wu, *Cryst. Growth Des.* **2019**
- (34) B.-W. Liu, M.-Y. Zhang, X.-M. Jiang, S.-F. Li, H.-Y. Zeng, G.-Q. Wang, Y.-H. Fan, Y.-F. Su, C. Li, G.-C. Guo, J.-S. Huang, *Chem. Mater.* **2017**, *29*, 9200-9207.
- (35) H. Lin, H. Chen, Y. J. Zheng, J. S. Yu, X. T. Wu, L. M. Wu, *Dalton Trans.* **2017**, *46*, 7714-7721.
- (36) H. Lin, L. Chen, J.-S. Yu, H. Chen, L.-M. Wu, *Chem. Mater.* **2016**, *29*, 499-503.
- (37) H. Lin, L. Chen, L. J. Zhou, L. M. Wu, *J. Am. Chem. Soc.* **2013**, *135*, 12914-12921.